1-1-2020

Hypervalent organoiodine(v) metal-organic frameworks: Syntheses, thermal studies and stoichiometric oxidants

Macguire R. Bryant
University of Wollongong, macguire@uow.edu.au

Christopher Richardson
University of Wollongong, crichard@uow.edu.au

Hypervalent organoiodine(v) metal-organic frameworks: Syntheses, thermal studies and stoichiometric oxidants

Abstract

This journal is © The Royal Society of Chemistry. Iodinated analogues of the highly porous IRMOF-9 and UiO-67 frameworks were prepared and post-synthetically oxidised with dimethyldioxirane (DMDO). Analysis by X-ray photoelectron spectroscopy (XPS) confirmed promotion to the iodine(v) state and detailed differential scanning calorimetry-thermal gravimetric analysis (DSC-TGA) showed the hypervalent metal-organic frameworks (MOFs) undergo exothermic elimination at ~200 °C with XPS showing hypervalency is maintained. The hypervalent MOFs are active heterogeneous reagents in sulfoxidation and alcohol oxidation reactions. The crystallinity and porosity of the MOFs were maintained following post-synthetic oxidation, thermolysis and after the heterogeneous reactions, as shown by powder X-ray diffraction (PXRD) and gas adsorption analyses. This work showcases the unique ability MOFs hold for studying chemical reactions and the potential for hypervalent organoiodine MOFs as reuseable oxidants.

Publication Details

Bryant, M. R. & Richardson, C. (2020). Hypervalent organoiodine(v) metal-organic frameworks: Syntheses, thermal studies and stoichiometric oxidants. Dalton Transactions, 49 (16), 5167-5174.

ARTICLE

Hypervalent Organoiodine(V) Metal-organic Frameworks: Syntheses, Thermal Studies and Stoichiometric Oxidants

Received 00th January 20xx,
Accepted 00th January 20xx

DOI: 10.1039/x0xx00000x

Macguire R. Bryant[a] and Christopher Richardson*[a]

Iodinated analogues of the highly porous IRMOF-9 and UiO-67 frameworks were prepared and post-synthetically oxidised with dimethyldioxirane (DMDO). Analysis by X-ray photoelectron spectroscopy (XPS) confirmed promotion to the iodine(V) state and detailed differential scanning calorimetry-thermal gravimetric analysis (DSC-TGA) showed the hypervalent metal-organic frameworks (MOFs) undergo exothermic elimination at ~ 200 °C with XPS showing hypervalency is maintained. The hypervalent MOFs are active heterogeneous reagents in sulfoxidation and alcohol oxidation reactions. The crystallinity and porosity of the MOFs were maintained following post-synthetic oxidation, thermolysis and after the heterogeneous reactions, as shown by powder X-ray diffraction (PXRD) and gas adsorption analyses. This work showcases the unique ability MOFs hold for studying chemical reactions and the potential for hypervalent organoiodine MOFs as reuseable oxidants.

[a] *School of Chemistry and Molecular Bioscience, University of Wollongong, Northfields Avenue, Wollongong, NSW 2522, Australia. E-mail: chris_richardson@uow.edu.au*

†Electronic Supplementary Information (ESI) available: Experimental details and ^{1}H and ^{13}C spectra of Me_2bpdc-I and H_2bpdc-I; Crystal structure tables and descriptions (CCDC 1953894-1953895). DSC-TGA, PXRD, FTIR and XPS data; gas adsorption isotherms and BET calculations. For ESI and crystallographic data in CIF or other electronic format see DOI: 10.1039/x0xx00000x

Introduction

Metal-organic frameworks (MOFs) are porous crystalline materials with a high degree of control over their structural and chemical features. Such control can be achieved through rational selection of the metal and organic components and by post-synthetic modification (PSM).[1, 2] The ability to engineer pore size, shape and functionality can be exploited to discriminate molecular species entering the pore structure and is where MOFS find applications as separators and heterogenous catalysts.[3]

Using the pores of MOFs to store and deliver reagents in stoichiometric or sub-stoichiometric chemical transformations has seen far less investigation than MOF-based catalysis.[4-7] However, MOF pores can be used as discrete domains to access novel reactivity,[8-15] and the ability to recover and reuse the MOF scaffold is beneficial in catalytic and in stoichiometric transformations.

A further possibility for MOFs is their potential as solid-state reaction matrices. This is where the framework backbone holds chemical groups rigidly in place with spatial separation. For instance, the immobilisation of catalysts on a framework scaffold avoids bimolecular catalyst deactivation pathways.[5] The immobilisation of metal complexes in MOF structures has facilitated photo-physical studies of their properties as isolated species,[16-18] and the capture of structural detail in catalytic processes by single crystal X-ray diffraction (SCXRD).[19] We have used MOFs as matrices for studying organic chemistry at temperatures above the decomposition points of the ligands themselves and established thermal methods as a gentle and efficient alternative for the PSM of MOFs.[20-24]

Dioxiranes are established as powerful and efficient oxygen transfer agents to promote organoiodine(I) to organoiodine(V).[25-29] We[30] and others[31, 32] have utilized dimethyldioxirane (DMDO) for quantitative post-synthetic oxidations of organic groups in MOFs. Here, we report the syntheses and detailed thermal studies of hypervalent iodo-functionalized analogues of IRMOF-9 and UiO-67 generated from post-synthetic oxidation using DMDO, and explore the materials as site-isolated heterogeneous oxidants on a MOF support.

Experimental Section

General procedures

All chemicals used were of analytical grade and purchased from either Sigma Aldrich, VWR Australia or Ajax Finechem Pty Ltd. ^{1}H NMR and ^{13}C NMR spectra were obtained using a Bruker Ascend NMR spectrometer operating at 400 MHz for ^{1}H and 101 MHz for ^{13}C. ^{1}H NMR spectra were referenced to the residual protio peaks at 2.50 ppm (d_6-DMSO) or 7.27 ppm ($CDCl_3$). ^{13}C NMR spectra were referenced to the solvent peaks at 39.6 ppm (d_6-DMSO) or 77.7 ppm ($CDCl_3$). For ^{1}H NMR analysis, zinc-based MOF samples (~5 mg) were digested by adding 35% DCl in D_2O (2 µL) and d_6-DMSO (500 µL), while zirconium-based MOF samples were digested in 96-98% D_2SO_4 in D_2O (5 µL) and d_6-DMSO (500 µL). In each case the samples were left until a solution was obtained.

Simultaneous differential scanning calorimetry-thermogravimetric analysis (DSC-TGA) data were recorded using a Netzsch STA449F3 at 10 °C/min under N_2 flow at 20 cm^3/min and compressed air 20 cm^3/min for activated MOF samples.

X-Ray photoelectron spectroscopy (XPS) was conducted using a SPECS PHOIBOS 100 Analyser installed in a high-vacuum chamber with the base pressure below 10^{-8} mbar. X-ray excitation was provided by Al Kα radiation with photon energy hν = 1486.6 eV (12 kV / 144 W). The XPS binding energy spectra were recorded at the pass energies of 20 eV and step width of 0.05-0.1 eV in the fixed analyser transmission mode. To increase the signal/noise ratio multi-scans conducted and the intensity of signals were accumulated. The broad survey scan was recorded at the pass energy of 60 eV and step width of 0.5. Analysis of the XPS data was carried out by using the commercial CasaXPS software package. All spectra were referenced to carbon at 284.8 eV.

Gas chromatography-mass spectrometry (GC-MS) chromatographs were obtained using a Shimadzu GC-2010 Plus fitted with a SH-Rxi-5Sil MS column (30 m x 0.25 µm x 0.25 µm) under He carrier gas flow (29.0 mL/min) and a Shimadzu AOC-20i/s Auto Sampler. Sample volumes of one µL in HPLC grade CH_2Cl_2 were injected in split mode (split ratio = 25:1) with the inlet temperature set to 280 °C. The initial oven temperature was set to 70 °C with a 1 minute equilibration time followed by a 45 °C/min ramp to 280 °C. The mass spectra were recorded on a Shimadzu GCMS-QP2020 Series with direct ionisation, with ion source temp set to 220 °C, interface temperature set to 280 °C and the mass range set to 40–750 *m/z* with 3.66 min scan time. The data was analysed using Labsolutions GCMS Solution v4.45 software, and compounds were identified by comparison with known compounds in the National Institute of Standards and Technology Mass Spectral database (NIST14 library).

Single crystal diffraction data were collected using a XtaLAB Mini II diffractometer with Mo Kα radiation (λ = 0.71073 Å) and a HyPix HPC detector. The data were integrated and scaled with CrysAlisPro 1.171.40.15 (Rigaku Oxford Diffraction, 2018) with empirical absorption correction using spherical harmonics, as implemented in SCALE3 ABSPACK scaling algorithm. The crystal structures were solved by direct methods using SHELXT[55] and refined against F^2 on all data by full-matrix least-squares with SHELXL[56] under Olex2.[57]

Powder X-ray diffraction (PXRD) patterns were recorded on a GBC-MMA X-ray diffractometer with samples mounted on 1" SiO_2 substrates. Experimental settings in the 2θ angle range of 3–30° with 0.02° step size and 1°/min scan speed were used for as-synthesised MOFs and 0.04° step size with 3°/min scan speed for activated MOFs post-oxidation.

Gas adsorption studies were carried out using a Quantachrome Autosorb MP instrument and high purity nitrogen (99.999%) gas at the Wollongong Isotope and Geochronology Laboratory. Surface areas were determined using Brunauer–Emmett–Teller (BET) calculations. Freeze

drying was carried out in a Christ Alpha 1-2 LDplus Freeze Dryer. Elemental microanalysis was performed by the Chemical Analysis Facility, Macquarie University, Australia.

Synthetic Procedures

$Zn_4O(bpdc\text{-}I)_3$

H_2bpdc-I (50.0 mg, 0.136 mmol) and $Zn(NO_3)_2{\cdot}6H_2O$ (123.2 mg, 0.414 mmol) were dissolved in DMF (4 cm^3) and placed in a screw-cap vial. The vial was capped and placed in an oven pre-heated to 100 °C for 18 hours to produce colourless, cubic-shaped crystals. The DMF solution was exchanged five times for fresh DMF at 100 °C, then at room temperature for CH_2Cl_2 over two days, and then for benzene over three days. The sample was activated by freeze drying for one hour then heating at 120 °C for five hours under vacuum. Found: C, 36.54%; H, 1.54%; N, 0.01%; $[Zn_4O(C_{14}H_7IO_4)_3]$ requires: C, 36.64%; H, 1.54%; N, 0.00%.

$Zr_6O_4(OH)_4(bpdc\text{-}I)_6$

In a screw-cap reaction vial, L-proline (125 mg, 1.09 mmol) and $ZrCl_4$ (50.6 mg, 0.217 mmol) were dissolved in DMF (2.5 cm^3) to which concentrated HCl (20 µL) was added dropwise with stirring. H_2bpdc-I (80.0 mg, 0.217 mmol) dissolved in DMF (2.5 cm^3) was added to the zirconium solution, and the reaction vial was capped and placed in an oven preheated to 120 °C for 24 hours to yield a white powder. The DMF solution over the precipitate was exchanged three times for fresh DMF at 120 °C, before being replaced with a solution of H_2bpdc-I (40.0 mg, 0.109 mmol) in DMF (5 cm^3) and placed in an oven preheated to 120 °C for 72 hours. The DMF solution over the precipitate was exchanged three times for fresh DMF at 120 °C, then at room temperature for CH_2Cl_2 over two days, then for acetone at 85 °C over one day, and then at room temperature for benzene over three days. The sample was activated by freeze drying for one hour then heating at 120 °C for five hours under vacuum. Found: C, 35.20%; H, 1.85%; N, 0.36%; $[Zr_6O_4(OH)_4(C_{14}H_7IO_4)_6]{\cdot}0.75C_3H_7NO{\cdot}0.85H_2O$ requires: C, 35.14%; H, 1.81%; N, 0.36%.

General Procedure for the Post-Synthetic Oxidations

$Zn_4O(bpdc\text{-}IO_x)_3$

A solution of cold, freshly prepared DMDO solution in acetone (3 cm^3, 0.24 mmol) was added to $Zn_4O(bpdc\text{-}I)_3$ (~20 mg, 0.015 mmol) under dry acetone (1 cm^3) in a screw-cap reaction vial. The vial was capped and left in a fridge set to 4 °C for 24 hours. NOTE: *Uncapping the vial and disturbing the solution can cause vigorous bubbling – caution should be taken in the following steps*. The DMDO solution was replenished and left for 24 hours after bringing the vial to room temperature. The solution over the now pale-yellow crystals was replaced with fresh dry acetone three times over 24 hours, CH_2Cl_2 over five days, then benzene over three days at room temperature. The sample was activated by freeze drying for one hour, before heating at 120 °C for five hours under vacuum. Found: C, 33.08%; H, 2.12%; N, 0.10%; $[Zn_4O(C_{14}H_9IO_7)_3]{\cdot}0.11C_3H_7NO{\cdot}H_2O$ requires: C, 32.74 %; H, 1.98%; N, 0.10%.

$Zr_6O_4(OH)_4(bpdc\text{-}IO_x)_6$

The same procedure was applied to $Zr_6O_4(OH)_4(bpdc\text{-}IO_x)_6$. $Zr_6O_4(OH)_4(bpdc\text{-}I)_6$ (~20 mg, 0.0078 mmol). Found: C, 30.34%; H, 2.25%; N, 0.00%; $[Zr_6O_4(OH)_4(C_{14}H_9IO_7)_6]{\cdot}8H_2O$ requires: C, 30.37 %; H, 2.25 %; N, 0.00%.

General Procedure for Oxidations with $Zr_6O_4(OH)_4(bpdc\text{-}IO_x)_6$

A portion of $Zr_6O_4(OH)_4(bpdc\text{-}IO_x)_6$ was added to a pre-weighed dry vial, heated to 100 °C for 15 minutes, and left to cool under vacuum for 30 minutes. The mass of the activated reagent was recorded. Dry $CHCl_3$ (500 µL) and trifluoroacetic acid in $CHCl_3$ solution (20 µL in 1 cm^3, 0.25 eq.) was added, and the suspension was stirred at room temperature for 30 minutes. Benzylalcohol, or thioanisole, in $CHCl_3$ solutions (20 µL in 1 cm^3, 0.25 eq.) was added to the stirred suspension, along with $CHCl_3$ to make the total reaction solution 1 cm^3 in volume. The vial was capped and placed into an oil bath preheated to 65 °C. For $Zr_6O_4(OH)_4(bpdc\text{-}IO_x)_6$, aliquots (20 µL) were taken at 0, 15, 30, 45, 60, 75 90, 120, 150, 180, 240, 300 and 360 minutes, added to a vial with a 1,2,4,5-tetramethylbenzene spike (0.06 mg/mL) in CH_2Cl_2 (HPLC grade, 980 µL) and analysed by GC-MS. R_T (min): thioanisole: 3.575; (methylsulfinyl)benzene: 4.491; (methylsulfonyl)benzene: 4.673; benzyl alcohol: 3.332; benzaldehyde: 3.025; 1,2,4,5-tetramethylbenzene: 3.694.

Results and Discussion

Ligand synthesis and oxidation

Dimethyl 2-iodo-[1,1'-biphenyl]-4,4'-dicarboxylate (Me_2bpdc-I) was synthesized by a method adapted from Olkhovik *et al.*[33] from dimethyl 2-amino-4,4'-biphenyldicarboxlate *via* a diazotization and iodination sequence. Hydrolysis of Me_2bpdc-I in aqueous base gave 2-iodo-[1,1'-biphenyl]-4,4'-dicarboxylic acid (H_2bpdc-I) in 94% isolated yield, which was characterized by microanalysis, NMR spectroscopy and electrospray ionisation (ESI) mass spectrometry. The structures of Me_2bpdc-I and H_2bpdc-I were determined by SCXRD (Table S2.1†, S2.2†, S2.3 and Fig. S2.1†, S2.2†). This revealed each molecule crystallized in the space group $P\bar{1}$ with one full molecule in the asymmetric units. H_2bpdc-I crystallizes as a solvate from DMSO solution with hydrogen bonding from a carboxylic acid group to a DMSO molecule disordered over two positions (occupancies 0.544(3) to 0.456(3)). Further descriptions of the structures and crystallographic data are provided in the ESI.

Treatment of Me_2bpdc-I in acetone with ~16 equivalents of DMDO in acetone solution at 4 °C overnight resulted in the formation of a microcrystalline product, according to powder X-ray diffraction (PXRD) (Fig. S4.3†), with a formula of Me_2bpdc-IO·H_2O. On reaction of Me_2bpdc-I with ~16 equivalents of DMDO in THF, colourless, needle-like crystals

were produced on slow evaporation. Unfortunately, these crystals were highly twinned, and we could not obtain definitive structural characterization from SCXRD analysis. Infrared spectroscopy showed a new band at 790 cm^{-1} that confirms the formation of an I=O bond (Fig. S3.1†, S3.2†).[34] Elemental analysis of the crystalline material was consistent with Me_2bpdc-IO·H_2O. For simplicity the material was termed Me_2bpdc-IO.

Similarly, reactions were performed on H_2bpdc-I in THF and in DMSO with DMDO in acetone. An amorphous precipitate with an elemental composition consistent with H_2bpdc-IO·THF formed on evaporation from THF. However, on slow evaporation from DMSO, clear, shard-like crystals were obtained, but these were also highly twinned, thwarting our attempts to determine the structure by single crystal diffraction methods. Infrared spectroscopy showed a band at 766 cm^{-1} signalling the formation of a I=O bond (Fig. S3.3†, S3.4†).[34]

MOF syntheses and post-synthetic oxidations

Based on literature procedures, H_2bpdc-I was used to prepare iodo-functionalized MOFs analogous to IRMOF-9[30] and UiO-67.[35] The linear biphenyl linkers bind to tetrazinc nodes and form interpenetrated cubic lattices in IRMOF-9, and coordination to the hexazirconium nodes in UiO-67-type structures results in a lattice featuring large octahedral and smaller tetrahedral pores (Fig. 1). Zn_4O(bpdc-I)$_3$ formed in DMF at 100 °C as large colourless cubic-shaped crystals using $Zn(NO_3)_2·6H_2O$ as the metal source, while $ZrCl_4$ was used to prepare $Zr_6O_4(OH)_4$(bpdc-I)$_6$ in a reaction modulated with concentrated HCl and L-proline at 120 °C in DMF, followed by an annealing step as outlined by Gutov *et al.*[36] PXRD patterns of Zn_4O(bpdc-I)$_3$ and $Zr_6O_4(OH)_4$(bpdc-I)$_6$ showed good agreement with the patterns of their parent IRMOF-9 and UiO-67 structures, respectively (Fig. S4.1†, S4.2†), confirming the MOF topologies.

Samples of Zn_4O(bpdc-I)$_3$ and $Zr_6O_4(OH)_4$(bpdc-I)$_6$ were solvent exchanged with acetone before treatment with excess DMDO (~16.5 eq. and ~76 eq., respectively) in acetone at 4 °C overnight, and then with fresh DMDO at room temperature for one day. The colours of the samples changed to an opaque pale yellow during these procedures.

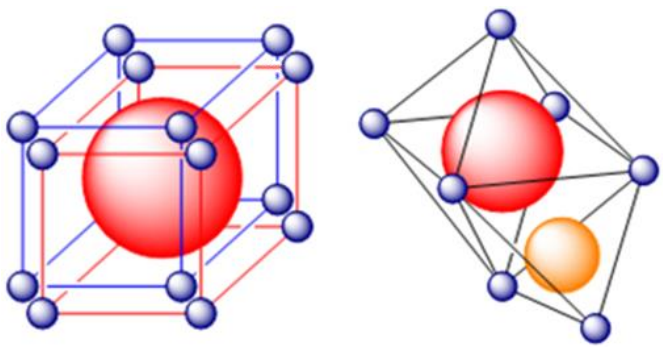

Fig. 1 Schematic structures of IRMOF-9 (left) and UiO-67 (right). The large red and yellow spheres are used to convey the pore space in the frameworks with the smaller blue spheres representing the metal nodes and the linking lines the linear bpdc-I bridging ligands.

X-ray photoelectron spectroscopic analysis

Binding energies of the iodine atoms in native and oxidised forms of the ligand, Zn_4O(bpdc-I)$_3$ and $Zr_6O_4(OH)_4$(bpdc-I)$_6$, along with iodoxybenzene (Ph-IO_2) as a positive control for an iodine(V) compound, were examined by X-ray photoelectron spectroscopy (XPS). Survey scans and fittings to the $I3_{d5/2}$ peaks of all compounds are shown in the ESI, with data for the MOFs and control compounds summarized in Table 1 and Fig. 2.

The data for H_2bpdc-I shows a single $I3_{d5/2}$ peak attributable to iodine(I) at 620.2 eV (Fig. 2a). We note here that this corresponds to the signal obtained from I_2.[37] The major signal in the spectrum of Ph-IO_2 at 623.4 eV corresponds to iodine(V), as expected (Fig. 2b). However, there is considerable signal intensity at 620.6 eV for iodine(I). It should be noted that organoiodine and hypervalent iodine compounds can decompose to I_2 during XPS analysis due to sample charging; Sherwood found signals corresponding to iodine(I) predominated, dependent on sample mounting, on XPS analysis of the I(V) compounds, iodic acid (HIO_3) at ~619.9 eV and anhydro-iodic acid (HI_3O_8) at 619.2 eV.[37] The purity of Ph-IO_2 was established by DSC-TGA (*vide infra*) so the signal at 620.6 eV is attributable to sample charging effects and not the presence of PhI, for example. Similarly, signals for iodine(III) at 622.1 eV and iodine(I) at 620.0 eV are evident in the XPS spectrum of the reaction product of H_2bpdc-I and excess DMDO (Fig. S8.6†). This product is free from the starting organoiodine(I) compound, H_2bpdc-I, and can be confidently assigned to the organoiodine(III) compound, H_2bpdc-IO.

A single signal in the XPS spectra of Zn_4O(bpdc-I)$_3$ and $Zr_6O_4(OH)_4$(bpdc-I)$_6$ is observed at 620.0 eV and at 620.2 eV, respectively, as expected for iodine(I) species (Fig. 2c, 2e). The XPS spectra of Zn_4O(bpdc-I)$_3$ and $Zr_6O_4(OH)_4$(bpdc-I)$_6$ after treatment with DMDO show peaks at 623.7 eV and 623.0 eV, respectively, consistent with iodine(V), and at 620.2 eV and 620.1 eV, respectively, for iodine(I) (Fig. 2d, 2f).[37]

Although the XPS analysis is complicated by sample charging effects, resulting in the generation or enhancement of a signal for iodine(I), we assert the oxidised forms of the MOFs are predominantly in the iodine(V) state, *vide infra*. As noted in the introduction, DMDO efficiently oxidises organoiodine(I) to organoiodine(V)[25, 27, 28] and the samples were exposed to 16 or more equivalents of DMDO in the oxidation procedure. For simplicity, the oxidised MOFs were named Zn_4O(bpdc-IO_x)$_3$ and $Zr_6O_4(OH)_4$(bpdc-IO_x)$_6$.

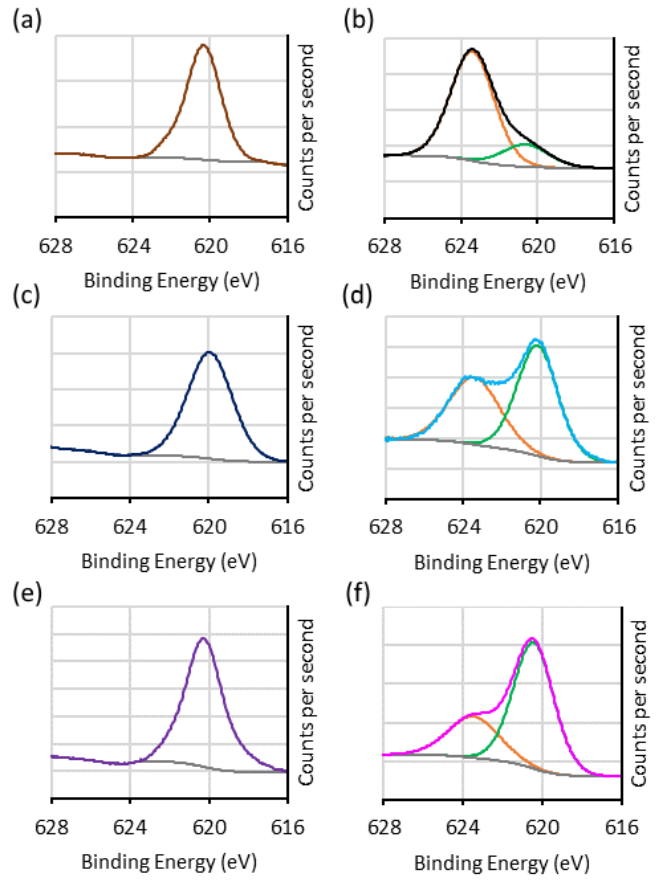

Fig. 2 XPS spectra of I $3_{d5/2}$ for (a) H_2bpdc-I, (b) Ph-IO_2, (c) Zn_4O(bpdc-I)$_3$, (d) Zn_4O(bpdc-IO_x)$_3$; (e) $Zr_6O_4(OH)_4$(bpdc-I)$_6$ and (f) $Zr_6O_4(OH)_4$(bpdc-IO_x)$_6$. Fittings for the baseline are shown in grey, iodine(I) in green and iodine(V) in orange.

Table 1. $I_{3d5/2}$ Binding energies from XPS analyses.

Material	Binding energies (eV)
H_2bpdc-I	620.2
H_2bpdc-IO	620.0, 622.1
Ph-IO_2	620.6, 623.4
Zn_4O(bpdc-I)$_3$	620.0
Zn_4O(bpdc-IO_x)$_3$	620.2, 623.7
$Zr_6O_4(OH)_4$(bpdc-I)$_6$	620.2
$Zr_6O_4(OH)_4$(bpdc-IO_x)$_6$	620.1, 623.0

Gas adsorption and surface area analysis

Powder X-ray diffraction (PXRD) analysis confirmed crystallinity was preserved for the post-synthetically oxidised MOFs, Zn_4O(bpdc-IO_x)$_3$ and $Zr_6O_4(OH)_4$(bpdc-IO_x)$_6$ (Fig. S4.1†, S4.2†). We have found that gas adsorption is a more sensitive measure of retention of pore structure than PXRD for MOF materials.[20-22, 24] Therefore, N_2 gas adsorption isotherms were recorded at 77 K on activated forms of Zn_4O(bpdc-I)$_3$, Zn_4O(bpdc-IO_x)$_3$, $Zr_6O_4(OH)_4$(bpdc-I)$_6$ and $Zr_6O_4(OH)_4$(bpdc-IO_x)$_6$ to fully analyse the effect of the PSM on the pore structure (Fig. 3).

Zn_4O(bpdc-I)$_3$ shows a Type I isotherm (Fig. 3a) with an uptake of 350 cm^3/g (STP), a pore volume of 0.52 cm^3/g and an apparent BET surface area of 1376 m^2/g. This compares well with IRMOF-9 (1918 m^2/g) and the isotopological diiodo-functionalized IRMOF-9, Zn_4O(bpdc-I_2)$_3$ (1184 m^2/g).[38] On oxidation, the surface area and pore volume reduce only slightly to 1220 m^2/g and 0.47 cm^3/g, respectively. The steep uptake at low pressures in the isotherm of Zn_4O(bpdc-IO_x)$_3$ and comparisons of the pore size distributions for native (9.6 Å,) and oxidised forms (7.9 Å and 10.0 Å) confirms the micropore structure is retained after the post-synthetic oxidation (Fig. 3a). It should be noted that IRMOF-9 itself possesses a bimodal pore structure (5.8 Å and 8.0 Å); however, ligand functionalization can block the small pores, resulting in an apparent monomodal pore structure.[38] The hysteresis present in the isotherm of Zn_4O(bpdc-IO_x)$_3$ indicates a small degree of mesoporosity brought about by the PSM, which we have observed before in post-synthetically modified IRMOFs.[21]

$Zr_6O_4(OH)_4$(bpdc-I)$_6$ displays an isotherm shape in accord with the parent UiO-67 MOF and related derivatives (Fig. 3b).[36, 39] The pore volume is 0.55 cm^3/g, and the accessible BET surface area is 1423 m^2/g. $Zr_6O_4(OH)_4$(bpdc-IO_x)$_6$ shows an isotherm shape and surface area comparable with its native analogue, with only a slight reduction in pore volume (Fig. 3b, Table 2). No hysteresis in the mesopore region is observed in the isotherm, and this is consistent with UiO-67 MOFs being more robust than IRMOF-9s.[40] As to be expected, the size of the pores in these iodo-functionalized UiO-67 materials (~8.5 Å) is smaller than those in UiO-67 (~11 Å)[41] due to the inclusion of the iodo groups in the framework. Both the surface area analysis and pore size results confirm the pore structures are nicely maintained upon post-synthetic oxidations with small and rational changes attributed to the size and mass of the included iodine substituents.

Table 2. Accessible BET surface areas and pore volumes of the MOFs from N_2 gas adsorption measurements at 77 K.

MOF	Accessible BET Surface Area (m^2/g)	Pore Volume (cm^3/g)
Zn_4O(bpdc-I)$_3$	1376	0.52
Zn_4O(bpdc-IO_x)$_3$	1220	0.47
$Zr_6O_4(OH)_4$(bpdc-I)$_6$	1423	0.55
$Zr_6O_4(OH)_4$(bpdc-IO_x)$_6$	1335	0.52

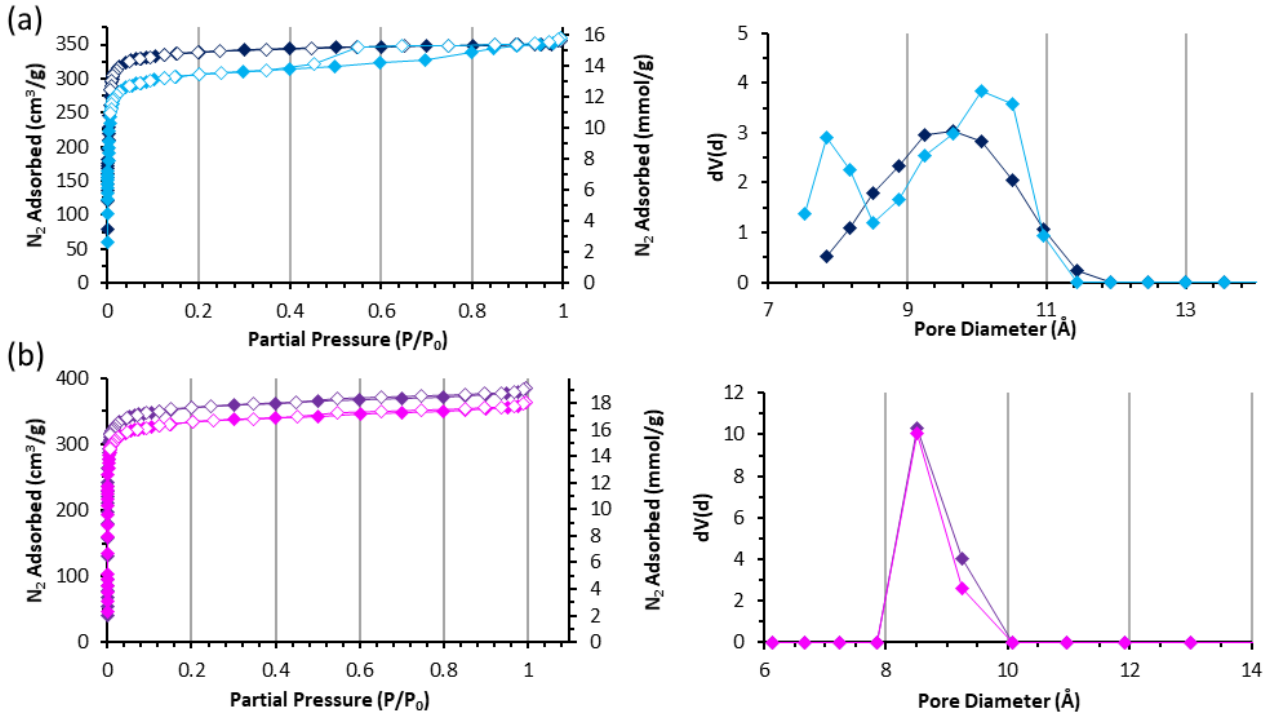

Fig. 3 N_2 sorption isotherms (left) and pore diameter distributions (right) of (a) $Zn_4O(bpdc\text{-}I)_3$ (dark blue), $Zn_4O(bpdc\text{-}IO_x)_3$ (light blue); (b) $Zr_6O_4(OH)_4(bpdc\text{-}I)_6$ (dark purple) and $Zr_6O_4(OH)_4(bpdc\text{-}IO_x)_6$ (magenta). Closed symbols represent adsorption, open symbols represent desorption; pore diameters derived from QSDFT equilibrium model kernel with slit/cylindrical pores.

Thermal analysis

The native and oxidised forms of Me_2bpdc-I, H_2bpdc-I and the MOFs were studied by simultaneous differential scanning calorimetry-thermogravimetric analysis (DSC-TGA, Fig. 4). The DSC-TGA trace of Me_2bpdc-I shows a melting event centred at 115 °C, and then a period of stability to 235 °C after which evaporative mass loss occurs. Me_2bpdc-IO_x does not melt but instead shows a violent exothermic event at 200 °C with a concurrent rapid loss of mass. Thermal analysis of H_2bpdc-I reveals no mass loss or thermal events until 327 °C, when the compound melts and then evaporates. Similar to Me_2bpdc-IO, the thermal analysis of H_2bpdc-IO reveals a rapid exothermic mass loss at 190 °C. The exothermic decomposition at approximately 200 °C in both oxidised materials is consistent with other hypervalent organoiodine compounds. For example, the iodine(III) compound iodosylbenzene (PhI-O) undergoes exothermic detonation at 210 °C,[42] while the iodine(V) compounds Ph-IO_2 (ESI, Fig. S6.5†)[43] and 2-iodoxybenzoic acid[44, 45] undergo exothermic detonations around 233 °C.

There are no mass losses coupled with thermal events in the DSC-TGA trace of activated $Zn_4O(bpdc\text{-}I)_3$ until decomposition above 400 °C. In contrast, the DSC-TGA trace of activated $Zn_4O(bpdc\text{-}IO_x)_3$ shows an exothermic mass loss at 200 °C (5.84%) and a smaller and broader exothermic mass loss centred at 260 °C (2.04%). Above this temperature a plateau of stability exists to around 400 °C, at which point decomposition starts (Fig. 4c). Activated $Zr_6O_4(OH)_4(bpdc\text{-}I)_6$ displays a similar DSC-TGA profile to $Zn_4O(bpdc\text{-}I)_3$, with no thermal events associated with mass losses until exothermic decomposition above 400 °C. $Zr_6O_4(OH)_4(bpdc\text{-}IO_x)_6$ displays two exothermic mass loss events, before undergoing framework decomposition around the same temperature as its native MOF. The exothermic mass loss events in $Zr_6O_4(OH)_4(bpdc\text{-}IO_x)_6$ are centred at 153 °C and 235 °C with a combined loss in mass of 10.88% (Fig. 4d). The composition of the hypervalent organoiodine groups in the MOFs was determined from the mass losses in TGA in combination with infrared spectroscopy and microanalytical data (Table S5.1†) to be -I=O$(OH)_2$, consistent with the XPS results for the iodine(V) oxidation state. Gas adsorption and PXRD measurements were made on each MOF after thermolysis reactions at 200 °C for one hour. The results showed the porosity of the zirconium MOF returned to a value close to the native material (Fig. S9.2) and was highly crystalline (Fig. S4.2), while the pore structure of the zinc MOF had collapsed (Fig. S4.1, S9.1, Table S9.1†). The latter result is related to the detonation of the sample when heated in >20 mg quantities. Furthermore, XPS analysis on the zirconium MOF post thermolysis showed no change to the I(I) to I(V) ratio.

The exothermic mass losses cannot be attributed to the evaporation of solvent trapped in the pores or bound to framework nodes, which are endothermic processes. A further analysis was to heat each of the oxidised MOFs to the plateau regions above the exotherms and then digest in deuterated acid and d_6-DMSO for analysis using solution phase ^{1}H NMR spectroscopy. In each case, the spectra revealed that bpdc-I was the sole product, indicating the mass loss is not associated with decomposition of bpdc-I (Fig. S6.1†). The NMR results

were supported by ESI mass spectra that returned only signals for H_2bpdc-I in each of the MOF digests (Fig. S7.1†).

Clearly, the exothermic events correspond to the thermal removal of the groups attached to the hypervalent organoiodine moieties in the MOFs. We sought to identify the eliminated fragments through TGA-MS techniques, however the results proved inconclusive.

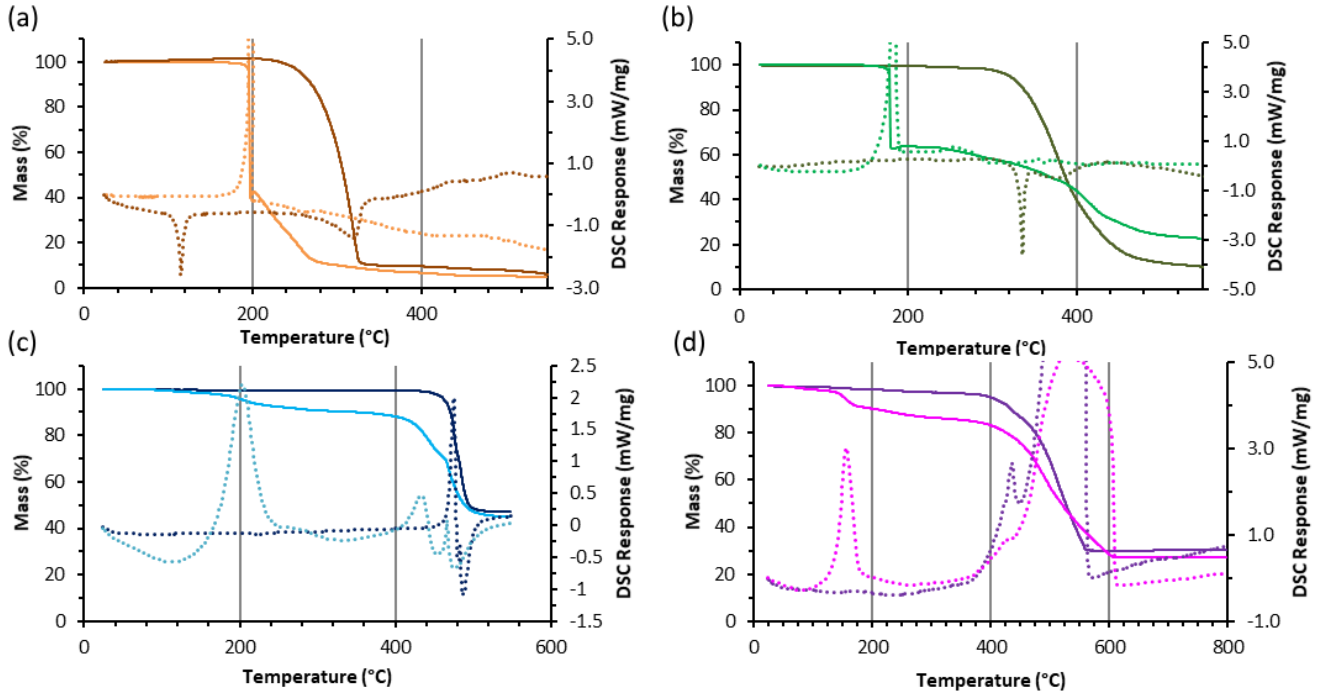

Fig. 4 DSC-TGA traces of (a) Me_2bpdc-I (dark orange), Me_2bpdc-IO_x (light orange); (b) H_2bpdc-I (dark green), H_2bpdc-IO (light green); (c) Zn_4O(bpdc-I)$_3$ (dark blue), Zn_4O(bpdc-IO_x)$_3$ (light blue); (d) $Zr_6O_4(OH)_4$(bpdc-I)$_6$ (dark purple) and $Zr_6O_4(OH)_4$(bpdc-IO_x)$_6$ (magenta). Solid traces represent the TG response, dotted traces represent the DSC response. Me_2bpdc-I, Me_2bpdc-IO_x, H_2bpdc-I, H_2bpdc-IO, Zn_4O(bpdc-I)$_3$ and Zn_4O(bpdc-IO_x)$_3$ were heated at 10 °C/min under a flow of N_2 (20 cm³/min); $Zr_6O_4(OH)_4$(bpdc-I)$_6$ and $Zr_6O_4(OH)_4$(bpdc-IO_x)$_6$ was heated at 10 °C/min under a combined flow of N_2 (20 cm³/min) and air (20 cm³/min).

Reagent Hypervalent MOF Oxidants

Iodine(III) and iodine(V) compounds are valuable classes of oxidant. Many such oxidants feature strong polymeric intermolecular bonding,[46] which inhibits dissolution in organic media.[47, 48] The presence of coordinating substituents *ortho* to organoiodine(V) sites greatly aids the solubility of these compounds by prohibiting such polymeric bonding. However, site isolation on a porous support would prevent intermolecular bonding and obviate solvent compatibility problems thereby expanding the scope of these oxidants.[49-51] Therefore, we forward the concept of a reusable hypervalent organoiodine MOF-based oxidant for stoichiometric conversions (Fig. 5). Examples of MOF-based reagents are rare but include the delivery of borane.[54] Here, this would involve 'charging' the iodo-functionality in the MOF to iodine(V) and 'discharging' as an oxidant in a separate reaction. Such an approach captures the benefits of performing transformations inside solid-yet-porous MOF scaffolds in terms of size-selective adsorption and facile separation of expired reagent from product *via* simple filtration. We reasoned a pore-based mechanism would predominate as the outer particle surfaces would passivate rapidly leaving the larger internal surface area hosting the iodine(V) groups. There has been interest in catalytic variants for organoiodine-functionalized MOFs in oxidation reactions.[53, 54]

As a proof of concept, we examined the sulfoxidation of thioanisole and the oxidation of benzyl alcohol with excess $Zr_6O_4(OH)_4(bpdc\text{-}IO_x)_6$ and a stoichiometric amount of trifluoroacetic acid in $CHCl_3$ at reflux. For comparison to a polymeric I(V) reagent, we employed Ph-IO_2 under the same reaction conditions. The oxidation of benzyl alcohol using Ph-IO_2 took 50 hours to reach completion and the oxidation of thioanisole did not proceed appreciably at all in the same time period (Fig S6.2, S6.3†). In contrast, the MOF-based oxidations were both complete in four hours according to GC-MS (Fig S10.1, S10.2†). No further oxidation to benzoic acid was observed in the oxidation of benzyl alcohol while a ~2:1 ratio of sulfoxide:sulfone was obtained in the oxidation of thioanisole. When these reactions were attempted using $Zr_6O_4(OH)_4(bpdc\text{-}I)_6$ there was no reaction, indicating the oxidations are not induced by a feature of the UiO-67 topology and can be attributed to the hypervalent organoiodine species. The crystallinity and porosity of the MOF samples were maintained after each reaction according to PXRD (Fig. S4.4, S4.5†) and gas sorption analysis (Fig. S9.2†). This highlights the potential for further development of reusable hypervalent organoiodine MOF-based reagents.

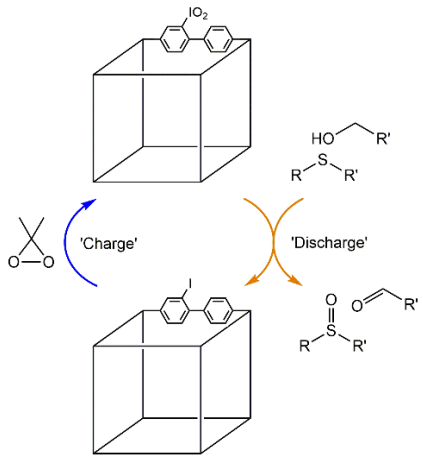

Fig. 5 Diagram of the MOF reagent concept, showing 'charging' of the MOF reagent and 'discharging' in an oxidation reaction.

Conclusions

Iodo-functionalized analogues of IRMOF-9 and UiO-67 are oxidised with DMDO to MOFs containing -I=O(OH)$_2$ groups as established by DSC-TGA, XPS, IR spectroscopy and microanalysis. The crystallinity and porosity of the MOFs were maintained after the post-synthetic oxidation. Lodging these groups in the MOF scaffolds allowed a rare study of their thermal properties, in which it was found that the hypervalent iodine groups undergo elimination without C-I bond fission or further decomposition. These hypervalent MOFs were active oxidants for sulfoxidation and alcohol oxidation. Our study sheds a new light on the thermal characteristics of organoiodine(V) compounds, and established the potential of hypervalent organoiodine MOFs as reusable stoichiometric oxidants.

Conflicts of interest

There are no conflicts to declare.

Acknowledgements

The authors acknowledge Dr Dongqi Shi for help obtaining XPS spectra. M. R. B. acknowledges the Australian Government for an Australian Government Research Training Program Award. C.R. thanks the University of Wollongong for financial support.

Notes and references

1 O. K. Farha and J. T. Hupp, *Accounts of Chemical Research*, 2010, **43**, 1166-1175.
2 D. J. Tranchemontagne, J. L. Mendoza-Cortes, M. O'Keeffe and O. M. Yaghi, *Chemical Society Reviews*, 2009, **38**, 1257-1283.
3 F. L. i. Xamena and J. Gascon, eds., *Metal Organic Frameworks as Heterogeneous Catalysts*, The Royal Society of Chemistry, Cambridge, 2013.
4 Y. Inokuma, G.-H. Ning and M. Fujita, *Angewandte Chemie International Edition*, 2012, **51**, 2379-2381.

5 Y. Inokuma, N. Kojima, T. Arai and M. Fujita, *Journal of the American Chemical Society*, 2011, **133**, 19691-19693.
6 Y. Inokuma, S. Yoshioka and M. Fujita, *Angewandte Chemie International Edition*, 2010, **49**, 8912-8914.
7 W. Choi, H. Ohtsu, Y. Matsushita and M. Kawano, *Dalton Transactions*, 2016, **45**, 6357-6360.
8 J. V. Knichal, H. J. Shepherd, C. C. Wilson, P. R. Raithby, W. J. Gee and A. D. Burrows, *Angewandte Chemie International Edition*, 2016, **55**, 5943-5946.
9 W. J. Gee, *Dalton Transactions*, 2017, **46**, 15979-15986.
10 T. Haneda, M. Kawano, T. Kawamichi and M. Fujita, *Journal of the American Chemical Society*, 2008, **130**, 1578-1579.
11 T. Kawamichi, T. Kodama, M. Kawano and M. Fujita, *Angewandte Chemie International Edition*, 2008, **47**, 8030-8032.
12 T. Kawamichi, Y. Inokuma, M. Kawano and M. Fujita, *Angewandte Chemie International Edition*, 2010, **49**, 2375-2377.
13 K. Ikemoto, Y. Inokuma and M. Fujita, *Journal of the American Chemical Society*, 2011, **133**, 16806-16808.
14 K. Ikemoto, Y. Inokuma, K. Rissanen and M. Fujita, *Journal of the American Chemical Society*, 2014, **136**, 6892-6895.
15 K. Ikemoto, Y. Inokuma and M. Fujita, *Angewandte Chemie International Edition*, 2010, **49**, 5750-5752.
16 A. J. Blake, N. R. Champness, T. L. Easun, D. R. Allan, H. Nowell, M. W. George, J. Jia and X.-Z. Sun, *Nature Chemistry*, 2010, **2**, 688.
17 T. L. Easun, J. Jia, J. A. Calladine, D. L. Blackmore, C. S. Stapleton, K. Q. Vuong, N. R. Champness and M. W. George, *Inorganic Chemistry*, 2014, **53**, 2606-2612.
18 T. J. Reade, T. S. Murphy, J. A. Calladine, R. Horvath, I. P. Clark, G. M. Greetham, M. Towrie, W. Lewis, M. W. George and N. R. Champness, *Philosophical Transactions of the Royal Society A: Mathematical, Physical and Engineering Sciences*, 2017, **375**, 20160033.
19 A. Burgun, C. J. Coghlan, D. M. Huang, W. Chen, S. Horike, S. Kitagawa, J. F. Alvino, G. F. Metha, C. J. Sumby and C. J. Doonan, *Angewandte Chemie International Edition*, 2017, **56**, 8412-8416.
20 A. D. Burrows, S. O. Hunter, M. F. Mahon and C. Richardson, *Chemical Communications*, 2013, **49**, 990-992.
21 L. Tshering, S. O. Hunter, A. Nikolich, E. Minato, C. M. Fitchett, D. M. D'Alessandro and C. Richardson, *CrystEngComm*, 2014, **16**, 9158-9162.
22 M. R. Bryant and C. Richardson, *CrystEngComm*, 2015, **17**, 8858-8863.
23 M. R. Bryant, T. A. Ablott, S. G. Telfer, L. Liu and C. Richardson, *CrystEngComm*, 2019, **21**, 60-64.
24 T. A. Ablott, M. Turzer, S. G. Telfer and C. Richardson, *Crystal Growth and Design*, 2016, **16**, 7067-7073.
25 A. Y. Koposov, R. R. Karimov, I. M. Geraskin, V. N. Nemykin and V. V. Zhdankin, *The Journal of Organic Chemistry*, 2006, **71**, 8452-8458.
26 D. F. Taber, R. A. Hassan and P. W. DeMatteo, *Organic Syntheses*, 2013, **90**, 350-357.
27 V. V. Zhdankin, A. Y. Koposov, D. N. Litvinov, M. J. Ferguson, R. McDonald, T. Luu and R. R. Tykwinski, *The Journal of Organic Chemistry*, 2005, **70**, 6484-6491.
28 U. Ladziata, A. Y. Koposov, K. Y. Lo, J. Willging, V. N. Nemykin and V. V. Zhdankin, *Angewandte Chemie International Edition*, 2005, **44**, 7127-7131.
29 V. V. Zhdankin, *The Journal of Organic Chemistry*, 2011, **76**, 1185-1197.
30 A. D. Burrows, C. G. Frost, M. F. Mahon and C. Richardson, *Chemical Communications*, 2009, 4218-4220.
31 31. K. Hindelang, A. Kronast, S. I. Vagin and B. Rieger, *Chemistry – A European Journal*, 2013, **19**, 8244-8252.
32 A. Kronast, S. Eckstein, P. T. Altenbuchner, K. Hindelang, S. I. Vagin and B. Rieger, *Chemistry – A European Journal*, 2016, **22**, 12800-12807.
33 V. K. Olkhovik, D. A. Vasilevskii, A. A. Pap, G. V. Kalechyts, Y. V. Matveienko, A. G. Baran, N. A. Halinouski and V. G. Petushok, *ARKIVOC*, 2008, **2008**, 69-93.
34 W. E. Dasent and T. C. Waddington, *Journal of the Chemical Society (Resumed)*, 1960, DOI: 10.1039/JR9600002429, 2429-2432.
35 R. J. Marshall, C. L. Hobday, C. F. Murphie, S. L. Griffin, C. A. Morrison, S. A. Moggach and R. S. Forgan, *Journal of Materials Chemistry A*, 2016, **4**, 6955-6963.
36 O. V. Gutov, M. G. Hevia, E. C. Escudero-Adán and A. Shafir, *Inorganic Chemistry*, 2015, **54**, 8396-8400.
37 P. M. A. Sherwood, Journal of the Chemical Society, Faraday Transactions 2: Molecular and Chemical Physics, 1976, **72**, 1805-1820.
38 R. Babarao, C. J. Coghlan, D. Rankine, W. M. Bloch, G. K. Gransbury, H. Sato, S. Kitagawa, C. J. Sumby, M. R. Hill and C. J. Doonan, *Chemical Communications*, 2014, **50**, 3238-3241.
39 M. J. Katz, Z. J. Brown, Y. J. Colon, P. W. Siu, K. A. Scheidt, R. Q. Snurr, J. T. Hupp and O. K. Farha, *Chemical Communications*, 2013, **49**, 9449-9451.
40 J. H. Cavka, S. Jakobsen, Unni Olsbye, Nathalie Guillou, Carlo Lamberti, Silvia Bordiga and K. P. Lillerud, *Journal of the American Chemical Society*, 2008, **130**, 13850-13851.
41 B. Wang, H. Huang, X.-L. Lv, Y. Xie, M. Li and J.-R. Li, *Inorganic Chemistry*, 2014, **53**, 9254-9259.
42 P. Müller and D. M. Gilabert, *Tetrahedron*, 1988, **44**, 7171-7175.
43 M. S. Yusubov, A. A. Zagulyaeva and V. V. Zhdankin, *Chemistry – A European Journal*, 2009, **15**, 11091-11094.
44 J. B. Plumb and D. J. Harper, *Chemical & Engineering News*, 1990, **68**, 3-3.
45 B. Janza and A. Studer, *The Journal of Organic Chemistry*, 2005, **70**, 6991-6994.
46 C. Wegeberg, C. G. Frankaer and C. J. McKenzie, *Dalton Transactions*, 2016, **45**, 17714-17722.
47 D. F. Banks, *Chemical Reviews*, 1966, **66**, 243-266.
48 E. B. Merkushev, *Russian Chemical Reviews*, 1987, **56**, 826.
49 N. N. Reed, M. Delgado, K. Hereford, B. Clapham and K. D. Janda, *Bioorganic & Medicinal Chemistry Letters*, 2002, **12**, 2047-2049.
50 R. R. Karimov, Z.-G. M. Kazhkenov, M. J. Modjewski, E. M. Peterson and V. V. Zhdankin, *The Journal of Organic Chemistry*, 2007, **72**, 8149-8151.
51 W.-J. Chung, D.-K. Kim and Y.-S. Lee, *Tetrahedron Letters*, 2003, **44**, 9251-9254.
52 X. Wang, L. Xie, K.-W. Huang and Z. Lai, *Chemical Communications*, 2015, **51**, 7610-7613.
53 B. Tahmouresilerd, P. J. Larson, D. K. Unruh and A. F. Cozzolino, *Catalysis Science & Technology*, 2018, **8**, 4349-4357.
54 A. D. Cardenal, A. Maity, W.-Y. Gao, R. Ashirov, S.-M. Hyun and D. C. Powers, *Inorganic Chemistry*, 2019, **58**, 10543-10553.
55 G. Sheldrick, *Acta Crystallographica Section A* **2015**, 71, 3-8.
56 G. Sheldrick, *Acta Crystallographica Section C* **2015**, 71, 3-8.
57 O. V. Dolomanov, L. J. Bourhis, R. J. Gildea, J. A. K. Howard, H. Puschmann, *Journal of Applied Crystallography* **2009**, *42*, 339-341.